

**RIBBON SCANNING CONFOCAL IMAGING FOR HIGH-SPEED HIGH
RESOLUTION IMAGING OF WHOLE TISSUES**

by

Annika H. Rose

B.A., Molecular & Cell Neurobiology / Cognitive Neuroscience

University of California, Berkeley, 2013

Submitted to the Graduate Faculty of
School of Medicine in partial fulfillment
of the requirements for the degree of
Master of Neuroscience

University of Pittsburgh

2016

UNIVERSITY OF PITTSBURGH

School of Medicine

This thesis was presented

by

Annika H. Rose

It was defended on

July 13, 2017

and approved by

Peter L. Strick, Thomas Detre Professor and Chair, Department of Neurobiology; Director,
Systems Neuroscience Institute; Scientific Director, University of Pittsburgh Brain Initiative

Simon C. Watkins, Distinguished Professor and Vice Chair, Cell Biology; Professor,

Immunology, Director, Center for Biologic Imaging

Robert S. Turner, Professor, Department of Neurobiology and Systems Neuroscience Institute

Thesis Director: Simon S. Watkins, Distinguished Professor and Vice Chair, Cell Biology;

Professor. Immunology. Director. Center for Biologic Imaging

Copyright © by Annika H. Rose

2017

RRIBBON SCANNING CONFOCAL IMAGING FOR HIGH-SPEED HIGH RESOLUTION IMAGING OF WHOLE TISSUES

Annika H. Rose, M.S.

University of Pittsburgh, 2017

In the past decade, there has been a growing interest in imaging whole brains in order to comprehensively map neural pathways that span the entire brain. Systems research at this scale has previously not been feasible, but due to technological and methodological advancements, many researchers have embraced this data-intensive, large-scale circuit mapping. Current approaches are limited by speed and/or resolution. In this paper, we describe a novel ribbon scanning confocal approach we use to image serial coronal sections of marmoset tissue. We show that this method surpasses the speed of current confocal approaches by at least ten times while obtaining equivalent subcellular resolution. Additionally, this new method virtually eliminates artifacts created by stitching together field of view tiles, generating a more seamless image. Finally, we go on to suggest this technology in the application of chemically cleared whole brains, using data from concurrent experiments.

TABLE OF CONTENTS

TITLE PAGE	i
COMMITTEE MEMBERSHIP PAGE	ii
ABSTRACT	iv
TABLE OF CONTENTS.....	v
LIST OF TABLES.....	vii
LIST OF FIGURES.....	viii
PREFACE.....	ix
1.0 INTRODUCTION.....	1
2.0 METHODS	4
2.1 ETHICS STATEMENT	4
2.2 ANIMALS AND SURGICAL PROCEDURES	4
2.3 TISSUE PREPARATION.....	6
2.4 MICROSCOPY.....	6
2.5 IMAGE RECONSTRUCTION	7
3.0 RESULTS	9
3.1 RIBBON SCANNING CONFOCAL MICROSCOPY IS A HIGH-SPEED HIGH-RESOLUTION MEANS OF ACQUIRING LARGE AREA MOSAICS	9

3.2	RIBBON SCANNING OF LARGE AREA SAMPLES IS FASTER THAN CONVENTIONAL HIGH-SPEED CONFOCAL MICROSCOPY WITH EQUIVALENT QUALITY AND REDUCED STITCHING ARTIFACTS	12
4.0	DISCUSSION	18
	APPENDIX A	22
	SUPPLEMENTAL EXPERIMENTAL PROCEDURES	22
	A.1.1 Injections of multi-synaptic wild type rabies virus.....	22
	A.1.2 Histology	23
	A.1.3 Image Acquisition	23
	APPENDIX B	25
	METHODS AND IMAGING OF LARGE VOLUMES OF CHEMICALLY-CLEARED TISSUE	25
	B.1.1 Ethics Statement.....	25
	B.1.2 Animals and Virus Infection.....	25
	B.1.3 Mouse Brain Tissue Preparation and CUBIC Clearing.....	26
	B.1.4 Microscopy.....	27
	B.1.5 Image Reconstruction.....	27
	B.1.6 Results	28
	BIBLIOGRAPHY	34

LIST OF TABLES

Table 1. Comparison of image scan times and pixel size	15
--	----

LIST OF FIGURES

Figure 1. The ribbon scanning approach.....	11
Figure 2. Ribbon scanning confocal microscopy is faster than conventional confocal microscopy but produces equivalent quality and reduced stitch artifacts.	13
Figure 3. Ribbon scanning demonstrates subcellular detail of a complete rat coronal section using 40x magnification..	14
Figure 4. Ribbon scanning confocal microscopy retains image quality and subcellular detail, while drastically reducing scan time.....	16
Figure 5. Confocal is more effective than 2-photon at multicolor deep tissue imaging in chemically cleared brains.....	29
Figure 6. Ribbon scanning confocal microscopy captures subcellular detail throughout large volumes in chemically cleared mouse brains.....	31
Figure 7. Multicolor large-volume imaging by ribbon scanning confocal microscopy	32

PREFACE

I would like to thank the members of the Center for Biologic Imaging for their sustained support throughout this project, particularly Greg Gibson, Callen Wallace, Morgan Jessup, and, most notably, Simon Watkins for his continued encouragement, advice and enthusiasm. I am forever grateful to Alan Watson, for his guidance, motivation, and collaboration on this project. Peter Strick was a pivotal mentor and advisor to me, and I thank him for helping provide the tools I needed to succeed and complete this project. I would like to acknowledge Elizabeth Wendel for her help and support. Finally, I would like to thank Mike Guest and Marcel Oberlaender for sharing tissue, data, and technical advice. Without the support of these people, I would not have been able to complete this project.

1.0 INTRODUCTION

In the late 1800's, Santiago Ramon y Cajal and Camillo Golgi birthed a scientific revolution like no other through their work in light microscopy and neuroanatomical tracing. Their efforts inspired neuronal tracing experiments and cell type investigations for decades to come, paving the way for advancements in circuit research critical to our current understanding of neuroanatomy (Cajal, 1891, 1893; De Carlos & Borrell, 2007). Even today, in the exploration of neural networks and circuit connectivity, neuroanatomical tract tracing represents the strongest tool for elucidating long-range and multi-synaptic connections. Traditional tracing methods involving the manual charting of individual labeled neurons using bright field microscopy and computerized plotting systems have generated key findings and fundamental insights into neural circuitry (Bostan, Dum, & Strick, 2013; Dum & Strick, 2003, 2013; Hoshi, Tremblay, Féger, Carras, & Strick, 2005; Kelly & Strick, 2003; Levinthal & Strick, 2012; Middleton & Strick, 2001). However, these manual techniques have proven to be, not only a major rate-limiting step in mapping connections, but also limiting in the scale of connectivity that can be measured.

Recent high-throughput connectomic initiatives aim to comprehensively map the neuroanatomical framework of model organisms in order to guide testable hypotheses about large-scale network function. Analyses at this scale have not previously been possible due to technological limitations, but revolutionary advancements have opened new doors to the future of systems research. Endeavors such as the Allen Brain Atlas, Brain Architecture Project, Mouse

Connectome Project, and Brain/MINDS project, to name a few, have begun to provide invaluable resources for this field of research (Bohland et al., 2009; Hintiryan et al., 2016; Majka et al., 2016; Oh et al., 2014; Okano & Mitra, 2015; Okano, Miyawaki, & Kasai, 2015; Zingg et al., 2014). These projects highlight long-range connectivity between major brain areas in several animal models, which can be used to inform future research. These extensive initiatives are able to succeed because of their innovative methodologies of digitization, visualization and computational analysis applied to entire brains. The traditional gold standard of eyepiece visualization is impractical for projects of this scale, which generate datasets at the magnitude of petabytes (Helmstaedter & Mitra, 2012). Consequently, researchers have turned to confocal microscopy as a new standard for the digital image capture of coronal sections of tissue.

The most time limiting step to collecting high resolution confocal images has been the collection of single two dimensional snapshots using a stop-and-shoot approach in which the stage is moved, the scanning is initiated, the image is collected and the process is repeated followed by image stitching. Even when using confocal systems with fast resonant scan heads the process remains slow, taking 2-5 seconds between positions. In addition, complex multipanel images are generally stitched on 3 axes, which takes significant time following collection. To satisfy Nyquist sampling, as resolution increases, the number of fields of view are essentially cubed according to the change in magnification and Z sampling, thus increasing the time it takes to acquire high-resolution volumes.

In this paper, we describe the application of a recently developed confocal technique that does not depend on the traditional “stop-and-shoot” approach. The system uses a resonant single axis scan head coupled to a fast stage that scans “ribbons” in a single movement. This allows large areas to be imaged in multiple colors very rapidly, collecting a 40,000*40,000 pixel mosaic

image in under 3 minutes as opposed to the 1.5 hours required using conventional confocal imaging. As stitching does not occur on the vertical axis, stitching artifacts are minimized and stitching speed is dramatically increased. The ultimate resolution using this method is exactly equivalent to other confocal methods, limited only by the wavelength of light used and the numeric aperture (NA) of the illumination/collection objective. We demonstrate the viability and speed of this system for scanning large areas of tissue in multiple colors, while retaining the sensitivity required to detect single infected neurons. While we are using this approach to gain insights into circuit mapping, its potential within imaging of all tissue samples is revolutionary when compared to other currently available technologies.

2.0 METHODS

2.1 ETHICS STATEMENT

In accordance with the University of Pittsburgh Institutional Animal Care and Use Committee guidelines, all animal procedures were performed under the approved protocol 12100628. All procedures used in these experiments were in accordance with the Association for Assessment and Accreditation of Laboratory Animal Care and the National Institutes of Health Guide for the Care and Use of Laboratory Animals. The experimental protocol was approved by both the Institutional Animal Care and Use Committee and the Biosafety Committee.

2.2 ANIMALS AND SURGICAL PROCEDURES

Three-year-old male common marmosets (*Callithrix Jacchus*) were obtained from Wisconsin National Primate Research Center. The marmosets were housed in an AAALACi accredited facility in Britz & Co. cages with approximately 4.2 sq ft cage space per quad. Housing rooms were maintained at 75-78 degrees F and a humidity range of 30-70%. Animals were fed a standard biscuit diet from Mazuri (Callitrichid Gel Diet # 5M16) with Vitamin D3 added. Fruits, vegetables, greek yogurt, acacia gum and protein supplements (crickets, mealworms and waxworms) were fed in addition to the standard diet.

Three-year-old male common marmosets (*Callithrix Jacchus*) were obtained from Wisconsin National Primate Research Center. The Marmosets were housed in an AAALACi accredited facility in Britz & Co. cages with approximately 4.2 sq ft cage space per quad. Housing rooms were maintained at 75-78 degrees F and a humidity range of 30-70%. Animals were fed a standard biscuit diet from Mazuri (Callitrichid Gel Diet # 5M16) with Vitamin D3 added. Fruits, vegetables, greek yogurt, acacia gum and protein supplements (crickets, mealworms and waxworms) were fed in addition to the standard diet. Marmoset were infected with the N2c strain of Rabies Virus (Matthias Schnell, Thomas Jefferson University) by injection in to the extensor digitorum communis muscle. The target muscle was exposed and identified by its origin and insertion, coupled with electrical stimulation (0.2-ms pulses at 25 Hz for 1 s, at a maximum intensity of 15 V). The animals were monitored at least twice daily prior to surgery and every 4-8 hours following surgery. During surgery, marmosets were anesthetized via inhalation of isoflurane 1-3% (vol/vol) with up to 5% for induction. On hour 117 following infection, euthanasia was carried out by anesthetizing the animals with isoflurane (3-5%) and then administering pentobarbitol (40mg/kg) IP. The animals were then administered three solutions by transcardial perfusion: (i) 0.1M phosphate buffer (pH 7.4), (ii) phosphate-buffered formalin (3.7 g of formaldehyde gas/100 ml of 0.1 M phosphate buffer), and (iii) a solution of 10% (vol/vol) glycerol in phosphate-buffered formalin at 4°C. 250-400ml of each solution. None of the marmosets showed severe signs of illness following infection or died without euthanasia.

2.3 TISSUE PREPARATION

Marmoset brains were sectioned using a vibratome into slices of 50 μ m thickness. Tissue sections were washed in PBS 3 times for 10 minutes each at room temperature. They were then blocked in a solution of 0.5% TritonX-100, 4% Normal Goat Serum (NGS) in PBS for 2 hours at room temperature. Following blocking, primary antibody was applied in a solution of 1% NGS, Rabbit anti-NeuN (Millipore 1:500), Mouse anti-Rabies (Matthias Schnell at Thomas Jefferson 1:50), and PBS for 48 hours at 4 degrees. The sections were again washed in PBS 3 times for 10 minutes each at room temperature. Next they were treated with secondary antibody in a solution of 3% NGS, 0.3% TritonX-100, Goat anti-Mouse IgG1 Alexa 488 (1:500), Goat anti-Rabbit IgG Alexa 647 and PBS for 2 hours at room temperature. Following secondary antibody, the tissue slices were washed again in PBS 3 times for 10 minutes at room temperature. They were then mounted on slides and allowed to dry. When dry, the slides were rinsed with ddH₂O and again allowed to dry. The slices were then coverslipped with cyto seal.

2.4 MICROSCOPY

Ribbon scanning microscopy was carried out on the beta RS-G4 confocal microscope purchased from Calibre I.D. Given the thin 50 μ m section of marmoset tissue, laser power ranged from 1-2%. Volumes were acquired with z-steps of 0.75 μ m with a lateral resolution per pixel of 0.356 μ m (Nikon 40x, 1.15NA, 0.6LWD, water), 0.551 μ m (Olympus 25x, 1.05NA, water), and 0.654 μ m (Olympus 20x, 0.7NA, air).

The resonant scanner frequency was 8000Hz with a pixel dwell time of between 30 and 100 nanoseconds. Two Hamamatsu photo multiplier tube detectors were used to detect emitted light from laser lines 488 (H13175U -110), 561 and 647 (H13175U -20). The pinhole size was 75 μ m (488) or 60 μ m (561, 647). Image frames were collected at 1024 x 1024 pixels at a rate of 5.9 frames per second. A Marzhauser Scanning stage SCANplus IM 120 x 80 (00-24-579-0000) was used to continuously move the samples under the scan head during ribbon acquisition. Z-alignment was based on the stage mechanics with an accuracy of 1 μ m and a minimum step size of 0.05 μ m. For a 3D stack, the stitch was calculated on the middle layer and applied to each subsequent layer, ensuring that each z-plane was assembled in precisely the same manner. Due to the speed of image collection, custom designed workstations were built for acquisition that included 64GB of RAM and four 1TB solid-state drives configured in RAID0.

The other confocal microscopes used in this study were a Nikon A1, Nikon A1R, and a Ti equipped with a Bruker (Bruker Scientific, Madison WI) Sweptfield Scanhead (now Opterra). In each case, the images were captured with a Nikon 20x, 0.75NA, air objective. In the case of the Nikon A1 images were collected with a 250nm point spacing, with the AR1 a 512x512 resonant image was collected with a zoom of 1x, with the sweptfield confocal images were collected using 512x512 Ander (Belfast Ireland) Ultra EMCCD camera, 50ms exposure time, 1x zoom.

2.5 IMAGE RECONSTRUCTION

Data storage and processing infrastructure was assembled for this project that included:

- 1) A high-speed file server with 160TB of raw storage capable of delivering 10 gigabits/s.

2) A computational server with dual Intel Xeon E5-2630 v3 processors, 512GB of RAM, dual NVIDIA GeForce GTX 1080 graphics and 32TB of solid-state drive storage configured in RAID0.

3) Numerous workstations were constructed that included an Intel i7-6850K processor, 128GB of RAM, NVIDIA GeForce GTX 1080 graphics, and 1TB of solid-state storage.

4) 10 gigabit networking was distributed to all systems.

3.0 RESULTS

3.1 RIBBON SCANNING CONFOCAL MICROSCOPY IS A HIGH-SPEED HIGH-RESOLUTION MEANS OF ACQUIRING LARGE AREA MOSAICS

Traditional large area mosaic imaging systems utilize a ‘stop-and-shoot’ modality that requires the sample to be precisely positioned for each mosaic field of view (FOV). This involves the initiation of mechanics that first move the sample and then manipulate shutter and laser positions for every tile within the mosaic. The sample is positioned so that each tile within the mosaic overlaps with adjacent tiles for computational joining (i.e. stitching) to form a single image. The oversampling required to collect this overlap can constitute up to 20-30 percent of the total image. In contrast to traditional ‘stop-and-shoot’ mosaic imaging systems, ribbon scanning confocal microscopy uses a continuous stage movement timed precisely to a high-speed resonance scanner (Fig. 1A). The microscope scans in vertical ‘ribbons’ where each image within the ribbon, comprised of a single FOVs, joins seamlessly (e.g. no overlap) along the x-axis. The absence of overlap within a ribbon eliminates the requirements for over sampling and the computational overhead required for stitching. During acquisition, the stage moves in a serpentine pattern under the scan head, pausing only momentarily at the completion of each ribbon to advance on the x-axis to the origin of a new ribbon. Each ribbon is acquired with overlap on one side resulting in an oversampling rate of approximately ten percent. With the

completion of each ribbon (Fig. 1B), the software initiates on-the-fly stitching with the adjacent ribbon, resulting in the near real time assembly of the final mosaic image (Fig. 1C). Each tile in the final mosaic represented one field of view from the objective (Fig. 1D) and resolved subcellular detail (Fig. 1E).

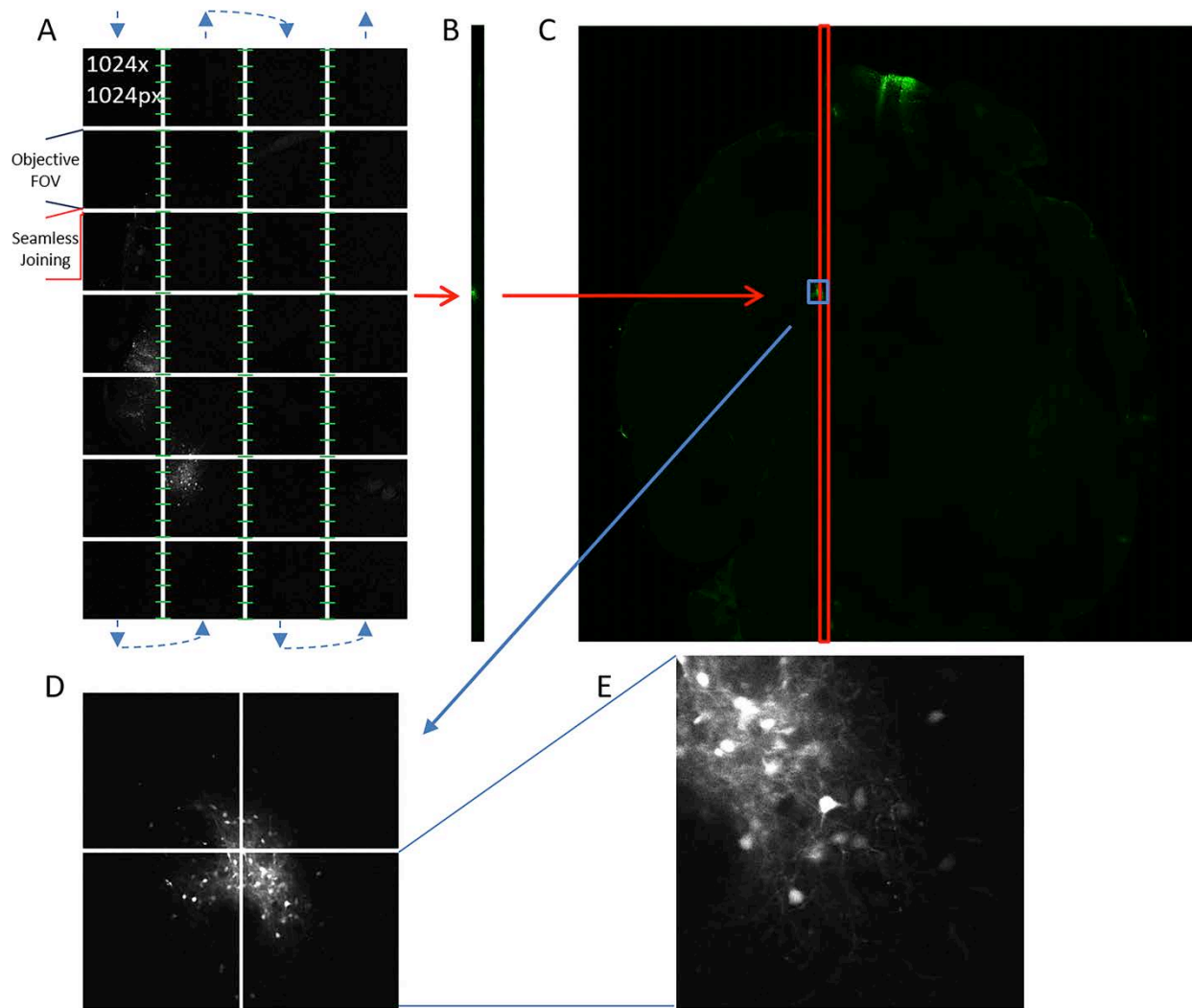


Figure 1. The ribbon scanning approach. (A) The blue arrows indicate the direction that the sample moves under the objective, acquiring non-overlapping individual fields of view, and pausing only at the end of each ribbon to advance on to the origin of the next ribbon. Each ribbon overlaps by ten percent with its adjacent ribbon. The overlap is used to stitch (green lines) each ribbon following its completion. (B) Completed ribbons are assembled into a (C) composite image that is representative of a single large-area scan. (D) Multiple fields of view elucidate regions or structures of interest within a larger area whereas each (E) individual field of view contains subcellular detail.

3.2 RIBBON SCANNING OF LARGE AREA SAMPLES IS FASTER THAN CONVENTIONAL HIGH-SPEED CONFOCAL MICROSCOPY WITH EQUIVALENT QUALITY AND REDUCED STITCHING ARTIFACTS

We compared the speed of ribbon scanning and commercial confocal microscopes for imaging large areas. Marmosets were infected with rabies virus and coronal sections were stained for virus proteins and with a nuclear marker. Using similar objectives, a 20 x 20mm area from a single section was imaged using ribbon scanning (Caliber I.D., Fig. 2A), a Nikon A1R (Fig. 2B) and a high-speed Nikon swept field confocal (Fig. 2C). All methods of image acquisition resulted in similar quality (Fig. 2D-F), effectively resolving subcellular details including cell bodies, axons and dendritic processes of infected cells. The subcellular detail was improved with ribbon scanning when viewed through a higher magnification objective (Fig. 3s). Ribbon scanning resulted in an improvement in the overall quality of the mosaic due to the reduced number of stitch seam artifacts (Fig. 2A). The ribbon scanning methodology improved the speed of acquisition by 413-fold compared to frame-by-frame based acquisition on the same system (Calibre I.D., Fig. 2G). The overall time to completion of a single mosaic was under 3 minutes by the ribbon scanning approach whereas the fastest comparable instruments, the Nikon A1R, Nikon A1 and Nikon swept field confocal (SFC) microscopes completed between 37-38 (Nikon A1R), 108 (Nikon A1), 210 (SFC simultaneous acquisition) and 1049 minutes (SFC sequential acquisition) (Fig. 2G). The quality of the images from the Nikon A1R and SFC microscopes were improved by using the Nikon A1, which uses a galvano scanner (Fig. 2H) or line averaging on the SFC (Fig. 2I), features not available on the Caliber I.D. ribbon scanning confocal. However, these methods of acquisition further increased the time of acquisition (Fig 2G).

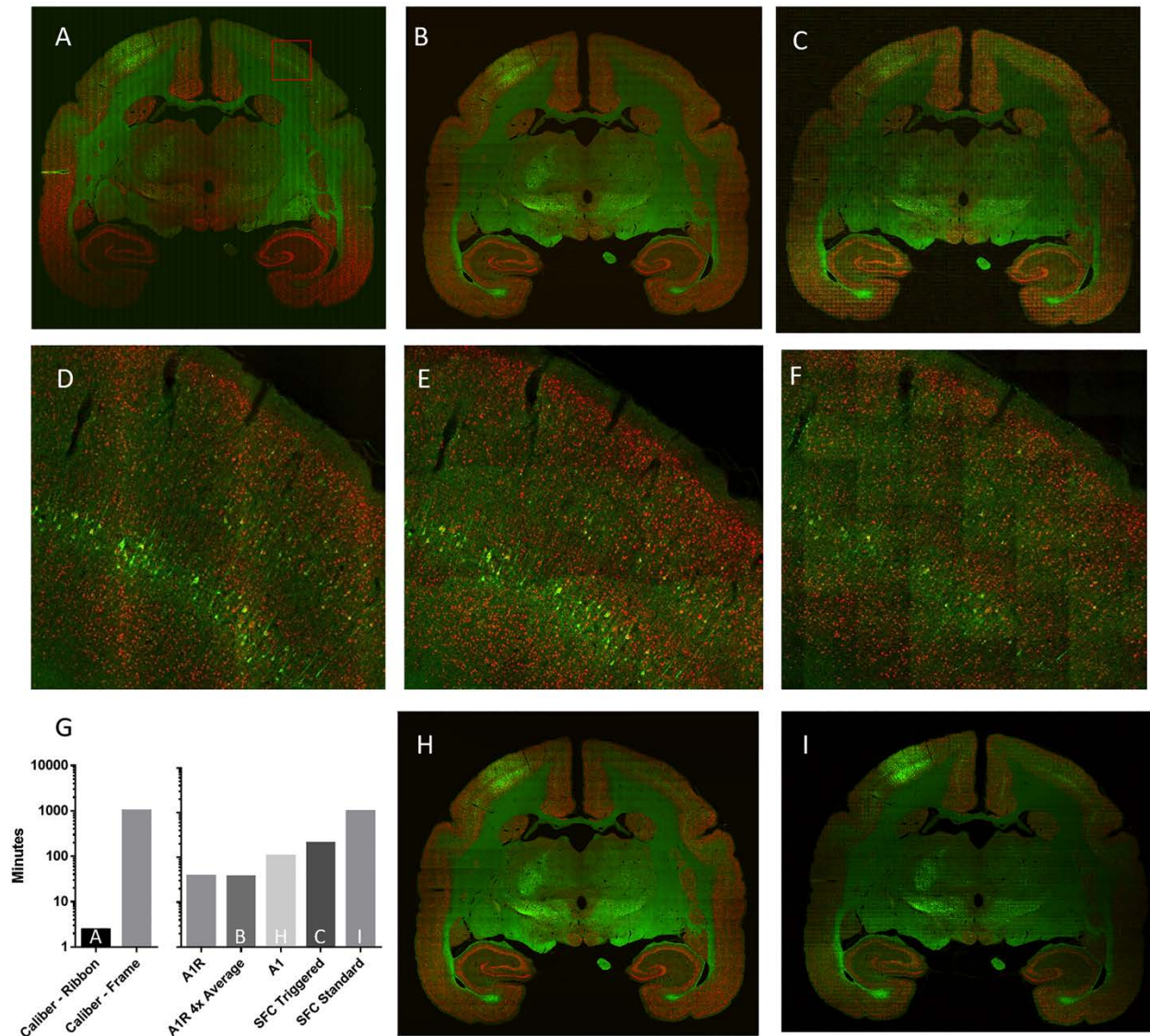


Figure 2. Ribbon scanning confocal microscopy is faster than conventional confocal microscopy but produces equivalent quality and reduced stitch artifacts. A single 20x20mm dry mount coronal section of marmoset brain was imaged on (A) the Caliber I.D. ribbon scanning confocal (Olympus 20x, 0.7NA) (B) the Nikon A1R using 4x averaging (Nikon 20x, 0.75NA) and (C) a swept field confocal using high-speed triggered acquisition (Nikon 20x, 0.75NA). Panels D-F are from the same zoomed regions of panel A-C, respectively. The times of acquisition for various microscopes and modes is recorded in panel G. Acquisition on a (H) Nikon A1 or (I) swept field confocal sequential acquisition led to better quality than the corresponding panels B and C but with additional time penalties. Note: some images were adjusted for background and contrast post-acquisition using Nis-Elements.

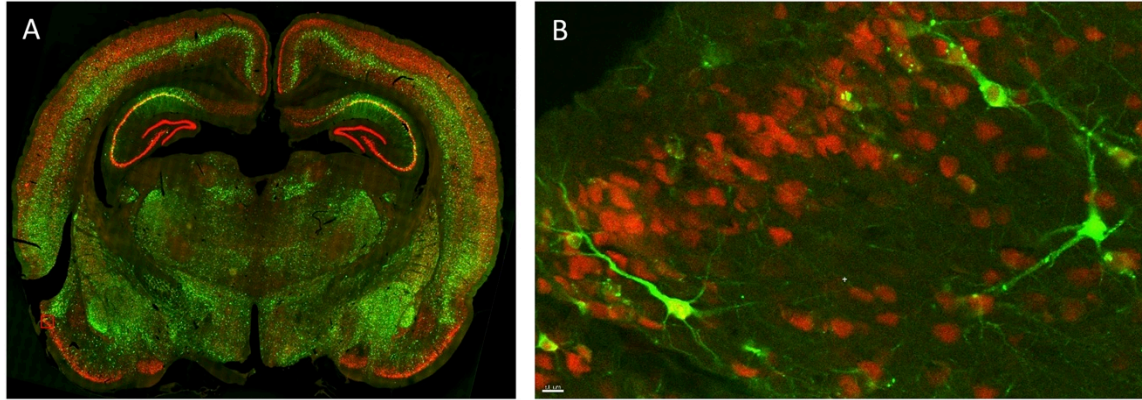


Figure 3. Ribbon scanning demonstrates subcellular detail of a complete rat coronal section using 40x magnification. (A) A whole coronal section of a rabies infected rat brain was stained for rabies (green) and nuclei (NeuN, red). (B) A zoomed image from panel A. The image was acquired by ribbon scanning using a Nikon 40x objective and a lateral per-pixel resolution of $0.363\mu\text{m}$.

We then performed a follow-up comparison on single plane rat brain tissue independently imaged by Mike Guest in the Oberlaender lab on a Leica confocal (Leica Application Suite Advanced Fluorescence SP5; Leica Microsystems) equipped with a resonance scanner. The average scan time per section was 10 minutes using a Leica 10x, 0.45NA, glycerol objective with a zoom of 1.7x. The tissue was shipped to Pittsburgh, where it was scanned on the ribbon scanning system using a Nikon 40x, 1.15NA, 0.6LWD, water objective, an Olympus 20x, 0.7NA, air objective and an Olympus 10x, 0.4NA, air objective, 1.7 zoom (results not pictured). The ribbon scanning system acquired images at up to 20 times the speed of the Leica system, using the 20x objective, and at 8 times the speed with 4 times the magnification using the 40x (Table 1). As shown previously, mosaic stitching artifacts were drastically reduced using the ribbon scanning approach (Fig. 4A-C, 4iii). Subcellular detail was maintained with the ribbon scanning system using the various objectives (Fig. 4i, ii, iv).

Table 1. Comparison of image scan times and pixel size

Microscope	Average Scan Time	Pixel Size
Leica (10x, 1.7 zoom)	10 minutes	0.868 x 0.868 x 1 μ m
Calibre (10x, 1.7 zoom)	1.15 minutes	0.67 x 0.67 x 1 μ m
Calibre (20x)	0.5 minutes	0.65 x 0.65 x 1 μ m
Calibre (40x)	1.25 minutes	0.36 x 0.36 x 1 μ m

While the 40x objective on the ribbon scanning microscope generated the crispest images (Fig. 4B), the time cost was inconsequential compared to the 10x when factoring in a zoom of 1.7 (Table 1). The 20x objective on the ribbon scanning system produced images of comparable quality (Fig. 3C) to the 10x Leica objective (Fig. 3A) in less than half the time. Traditionally, images have been collected at 10x only because any magnification greater than that is not feasible for whole-brain or large-scale investigations on commercially available confocal microscopy systems.

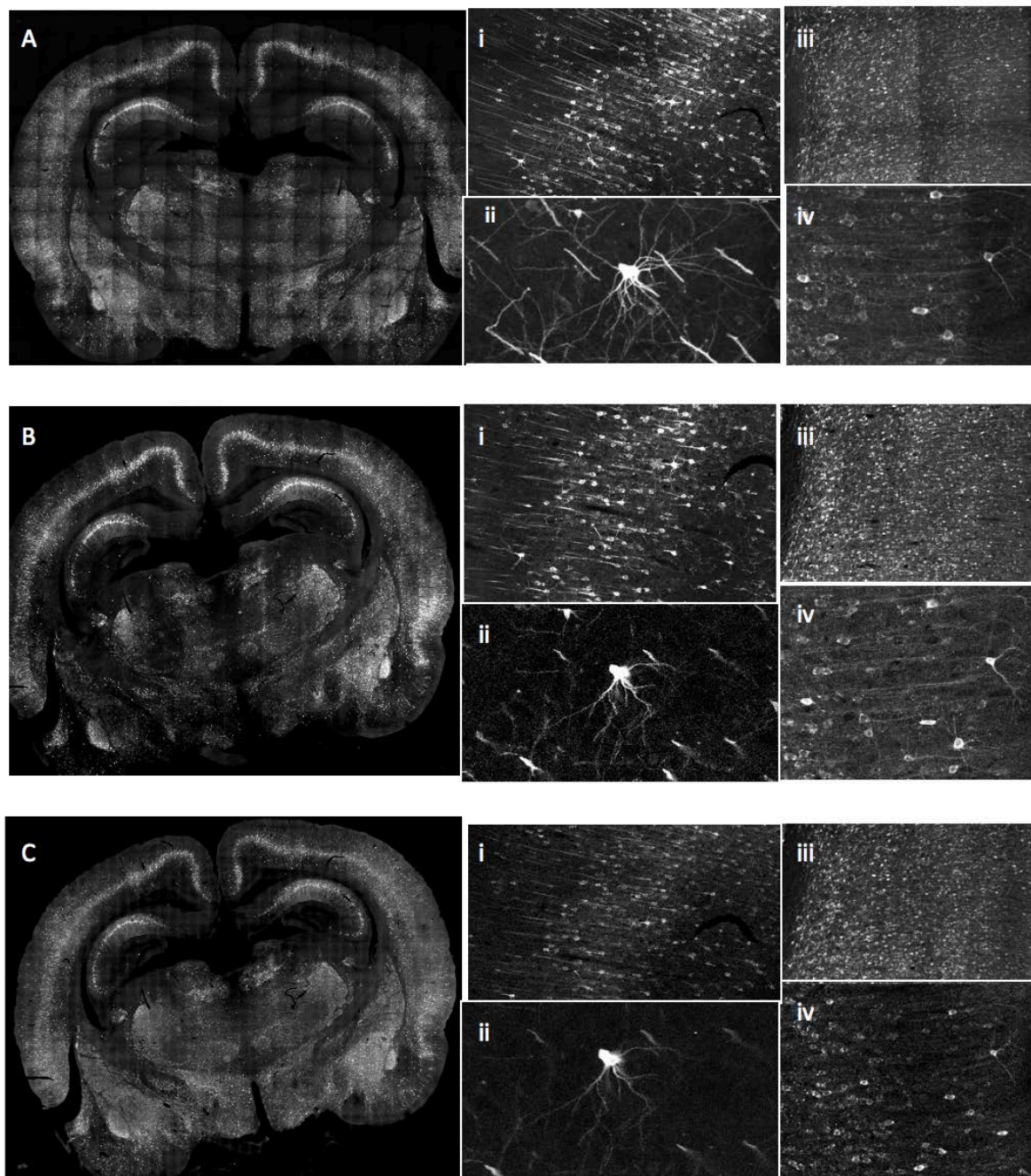


Figure 4. Ribbon scanning confocal microscopy retains image quality and subcellular detail, while drastically reducing scan time compared to other confocal microscopy. Coronal sections from a rat brain were imaged using (A) a Leica confocal microscope with a Leica 10x, 0.45NA, glycerol objective and a 1.7x zoom and the ribbon scanning system with no zoom and (B) a Nikon 40x, 1.05NA, LWD water objective and (C) an Olympus 20x 0.7NA, air objective. (A-Ci-iv) Zoomed regions are shown for each whole-brain image. Note: no post-processing adjustments were made.

Imaging entire marmoset coronal sections in three dimensions to transverse the entire 50 μ m section requires 17-21 Z-stacks per section, which is a hugely time-consuming process with standard confocal laser scanning microscopy (CLSM) systems, with some scans lasting greater than 24 hours, even with a 10x objective. A significant portion of that time is devoted to mosaic stitching. The rate-limiting factor in traditional confocal microscopy is the speed of the galvanometer mirrors, which are linearly controlled and average 4 frames per second. Alternatively, non-linear resonant scanning mirrors oscillate at a fixed rate and allow for high-speed image capture of up to 30 frames per second with the tradeoff of lower resolution. This significantly cut down on scan time (from 20-24 to about 10-15). SFC microscopy allows for an increase from 30 frames per second to 1200 frames per second using a 50 μ m slit aperture. Using a Nikon 20x, 0.7NA air objective, 0.32 μ m/pixel resolution was achieved over a scan time of 8-10 hours, while a 10x objective cut scan time down to 3-5 hours with a resolution of 0.66 μ m/pixel. The post-processing steps of shading corrections, dust removal, background subtraction, and large image composition on average lasted 2-4 hours. Given the drastic decrease of scan time of the custom SFC system, this accounted for approximately half of the total scan time.

In comparison, the ribbon scanning system, can acquire the same number of z-stacks in approximately 30 minutes with a similar 20x objective. One reason for this efficiency is that stitching seams are effectively eliminated in the horizontal plan, as indicated in Fig. 2 and 3, and mosaic stitching no longer constitutes a significant percentage of scan time.

4.0 DISCUSSION

Here we demonstrate the potential of ribbon scanning confocal microscopy to rapidly image whole brain tissue sections at subcellular resolution. This approach increases the speed of large-area confocal microscopy by at least a factor of 10 when compared to commercially available systems. The lack of tradeoff between speed and resolution make it a powerful tool for investigations at the scale. We suggest that the speed and utility of this approach (when applied to the brain and other organs) makes it broadly applicable to the study of infectious disease, gene expression, developmental biology and neurobiology.

While confocal methods allow exquisite reconstructions of small tissue regions extending the method to the whole brain has proven quite difficult and extremely time consuming. With the speed and efficiency of this ribbon scanning approach, the imaging of serial coronal sections of fixed tissue of entire brains is now a much more feasible feat. The large-scale initiatives using this chosen method could benefit significantly from implementing this technology. However, it still remains time consuming and potentially hindering to reconstruct vast datasets, with an estimated 200-300 50 μ m sections per brain, each consisting of 15-25 z-planes. While manual quantification remains the gold standard, it is necessary to incorporate automated workflows for pre- and post- processing in order to map connections at this scale.

There are a number of computational realignment methods that aim to re-align serial sections into a three-dimensional virtual brain using a series of two-dimensional rigid and three-

dimensional affine transformations to address issues of tissue distortion, shrinkage, and irregularities that occur during sectioning and histological processing. Once aligned, three-dimensional deformable registration tools are used to warp the virtual brain to a reference brain (Majka et al., 2016). However, many of these algorithms are tailored towards imaging methods such as STP tomography, which images sections with a multiphoton microscope as they are cut via microtome, eliminating the potentially confounding steps of staining and mounting. In addition, manual manipulations and adjustments at one or more stages of the process are still necessary and can constitute a substantial portion of time given the number of sections. Finally, with these transformations, a new set of problems presents itself, which is that of the reconstruction of continuous neuronal processes. Sectioning severs axons, dendrites, and cell bodies, making a complete reconstruction a challenge if not impossible. Even with modern algorithms, many if not most neurons remain disjointed, especially when mounted and imaged.

At every level of resolution, from the single neuronal synapse to the anatomically isolated but interconnected functional compartment, there is a fundamental need to define complexity as a continuum such that cell development, position, interaction, and death are understood within the context of the neighboring cells and anatomical landmarks. Because of this, many research groups working at this scale have turned to chemically clearing tissue and imaging entire volumes. Recent advances in tissue clearing approaches have allowed imaging at great depths, making the third dimension obtainable and enabling imaging of whole brains (Sca/e (Hama et al., 2011), CLARITY (Chung et al., 2013) , CUBIC (Susaki et al., 2014a) and DISCO (3 (Becker, Jährling, Saghaei, Weiler, & Dodt, 2012a), i (Renier et al., 2014a), u (Pan et al., 2016a)).

The main skepticism of imaging cleared tissues is resolution. For example, one of the most popular methods for imaging cleared tissue is light sheet microscopy. Light sheet methods,

in which the sample is illuminated laterally with a thin sheet(s) of light, allow rapid collection using sCMOS detectors. Generally, a relatively low resolution overview is acquired which is used to guide collection of a higher resolution subimage, with a different objective or intermediate zoom optics (for example the LaVision system). However, this method demands complex sample mounting approaches and minimization of the refractive index change across the sample. Ultimately, there is a significant compromise in Z-resolution due to the inherent and somewhat variable thickness of the illuminating light sheet, and the XY resolution is limited to a circumscribed choice of collection optics.

Using this ribbon scanning technology, we have shown significant advantages for imaging cleared tissues compared to other imaging methods (See Appendix C). In addition to the compelling advantage of speed of imaging, sample preparation and mounting is trivial compared to light sheet methods. Furthermore, the pinhole aperture of the ribbon scanning system limits the collection of out-of-focus light, reducing discrepancies between refractive indices and allowing for higher resolution in deep tissue. Finally, the ribbon scanning microscope reduces damage by photobleaching due to the high-speed resonant scanner limiting exposure of the tissue to light. Each pixel is exposed to the laser for a maximum of 100ns.

With the advent of ribbon scanning technology, the rapid collection of large area confocal data sets is now accessible. Ribbon scanning technology is as high-resolution and flexible as confocal imaging systems with the speed of wide field imaging systems that are used on light-sheet microscopes. This combination is a powerful tool that enables the more complete collection of large-area / large-volume data sets that could range from live cells to whole animals on a single platform. We expect that the ribbon scanning confocal system will be more cost effective for researchers since the speed of acquisition will enable the collection of multiple whole tissues

or organisms in a single day. Additionally, we expect that a complete ribbon scanning system (once commercially available) is likely to be 3-4 times less than currently available light-sheet solutions. The expected affordability coupled with the rapid acquisition of data will elevate subcellular imaging of whole tissues and organisms to a principal means of experimental evaluation and perhaps into the toolbox of fields unrelated to neuroscience.

APPENDIX A

SUPPLEMENTAL EXPERIMENTAL PROCEDURES

The following methods were performed by Mike Guest with help from Elizabeth Wendel to obtain the rat brain tissue described in Section 3.2.

A.1.1 Injections of multi-synaptic wild type rabies virus

All experimental procedures were carried out at the University of Pittsburgh, after evaluation by a local ethical committee (IACUC) and in accordance with the animal welfare guidelines of the NIH. Young adult (P28-P35) male Wistar rats were anesthetized with a ketamine-xylazine mixture (70 / 6 mg/kg, i.p.) and placed in a stereotaxic frame (Helmut Saur Laboratories). The rat's head was rotated 20 degrees upwards in the ventral/dorsal direction to give better visual access to the right whisker pad on the snout. The C3 whisker was identified visually under a stereoscope (Leica MZ6) and marked at the base of the snout with a surgical pen. The fur surrounding the targeted whisker was trimmed away and a small incision next to the target whisker follicle was made. A steel injection needle attached to a 5 μ m glass Hamilton syringe was inserted into the incision approximately 1mm below the skin of the whisker pad using a manual micromanipulator (Narishige Model BE-8). 500 to 700nL of wildtype rabies virus

(Thomas Jefferson University, 5×10^8 PFU) was then pressure injected into the targeted whisker follicle under visual control. Rats underwent survival periods of 3 days to 5 days in order to establish the rate of rabies virus transport.

A.1.2 Histology

Rats were perfused transcardially with phosphate buffer, and brains were removed and fixed with paraformaldehyde. They were then blocked in 10% gelatin and fixed in 4% PFA overnight. Consecutive 50 μ m thick vibratome slices were cut coronally through the entire brain. For rats injected with rabies virus, slices were double-immunolabeled to visualize and count rabies labeled cells with respect to all neurons (NeuN). To do so, slices were permeabilized and blocked in 0.5% Triton x-100 (TX) (Sigma Aldrich) in 100mM Phosphate Buffer (PB) containing 4% normal goat serum (NGS) (Jackson ImmunoResearch Laboratories) for 2hrs at room temperature. Primary antibodies were diluted 1:500 (Rabbit anti-NeuN, EMD Millipore #MAB377) and 1:1000 (Mouse anti-Rabies, Thomas Jefferson University) in PB containing 1% NGS for 48 hours at 4°C. Secondary antibodies (1:500 goat anti-mouse IgG Alexa-488 and 1:500 goat anti-Rabbit Alexa-647) were incubated for 2-3 hours at room temperature in PB containing 3% NGS and 0.3% TX. All slices were mounted on glass slides, embedded with SlowFade Gold (Invitrogen) and enclosed with a cover slip.

A.1.3 Image Acquisition

All images were acquired using either a confocal laser scanning system (Leica Application Suite Advanced Fluorescence SP5; Leica Microsystems) equipped with glycerol/oil immersion

objectives (HC PL APO 10x .04 N.A., HC PL APO 20x .7 N.A., and HCX PL APO 63x 1.3 N.A.), a tandem scanning system (Resonance Scanner), spectral detectors with hybrid technology (GaAsP photocathode) and mosaic scanning software (Matrix Screener, beta version provided by Frank Sieckmann, Leica Microsystems). For quantification of labeling in rabies injection experiments (Rabies-488, NeuN-647), dual channel mosaic scans of areas of the entire brain were acquired using a 10x glycerol objective at a resolution of $0.868\mu\text{m} \times 0.868\mu\text{m}$ per pixel (1.7x digital zoom, 8x line average, 8-kHz scanning speed. For single neuron reconstruction of rabies labeled neurons, single channel mosaic image stacks of volumes up to $1 \times 1 \times 0.05\text{mm}$ were acquired using a 63x glycerol objective at a resolution of $0.092 \times 0.092 \times 0.5\mu\text{m}$ per voxel (2.5x digital zoom, 8x line average, 8k-Hz scanning speed, 13 x 13 fields of view). For quantification of NeuN-Alexa647 labeled cells, single channel mosaic image stacks of volumes up to $3 \times 1.5 \times 0.05\text{mm}$ were acquired using a 20x glycerol objective at a resolution of $0.361 \times 0.361 \times 1\mu\text{m}$ per voxel (2.0x digital zoom, 8x line average, 8k-Hz scanning speed, 10 x 6 fields of view).

APPENDIX B

METHODS AND IMAGING OF LARGE VOLUMES OF CHEMICALLY-CLEARED TISSUE

Most experimental and clearing procedures pioneered and spearheaded by Alan Watson, with help from Greg Gibson and myself.

B.1.1 Ethics Statement

All animal procedures were carried out in accordance with University of Pittsburgh Institutional Animal Care and Use Committee guidelines under the approved protocol 15076006.

B.1.2 Animals and Virus Infection

CD1 Mice were ordered at six weeks of age from Charles River and were housed under the same environmental conditions as rats. The mice were infected at ABSL-3 within the University of Pittsburgh Regional Biocontainment Laboratory. Virus was introduced subcutaneously in a single rear footpad with $1e03$ PFU of Venezuelan equine encephalitis virus (VEEV) expressing mCherry. mCherry was inserted into the V3000 of the Trinidad Donkey strain of VEEV (VEEV

TrD TaV-cherry) as previously described (Sun, Gardner, Watson, Ryman, & Klimstra, 2014). GFP was inserted into the western equine encephalitis Virus (WEEV) McMillian strain (WEEV McM TaV-GFP) as previously described (Sun et al., 2014). Aerosol infections were completed with WEEV McM TaV-GFP and the FL93-939 strain of eastern equine encephalitis virus expressing GFP (EEEV TaV-GFP) (Sun et al., 2014). Virus was produced from infectious clones and tittered as previously described (Sun et al., 2014). Aerosol exposure of mice was conducted using the AeroMP (Biaera technologies, Hagerstown, MD) (Reed, Bethel, Powell, Caroline, & Hartman, 2014). Mice were euthanized at 72-96 hours post infection and perfused transcardially with PBS and then 4% PFA or 4% PFA containing 20nm yellow-green fluorescent beads (Thermo Fisher, F8787). Brains were fixed in 4% PFA at 4 degrees Celsius for 24 hours prior to removal from ABSL-3 containment.

B.1.3 Mouse Brain Tissue Preparation and CUBIC Clearing

Mouse brains were incubated overnight at 4 degrees Celsius in hydrogel solution (Chung et al., 2013) in DPBS and without PFA (4% acrylamide, 0.05% bis-acrylamide, 0.25% VA-044). The hydrogel was polymerized by shifting the brains to 37 degrees Celsius for 4 hours. Brains were then horizontally sectioned with a razor blade to a thickness of approximately 4mm to include the olfactory bulb. The sections were cleared using CUBIC (Susaki et al., 2015) by immersion in 50% CUBIC R1 for 1 day, then the solution was changed to 100% CUBIC R1 on days 2, 3, 7 and 10. Incubations were completed at 37 degrees Celsius with gentle movement. The cleared tissue was mounted in CUBIC R1 for imaging.

B.1.4 Microscopy

Ribbon scanning microscopy was completed on the pre-commercial RS-G4 confocal microscope purchased from Caliber I.D. Large-area mosaic images were captured using either the ribbon-scanning or frame modes. Laser powers used for imaging varied for each tissue and depth of each optical section but were approximately 15-30% for deep tissue imaging of mouse brains (dependent on depth). Most volumes were acquired with Z-steps of 25.15 μM to impose practical limits on the scale of the data collected (under these conditions, our largest dataset was approximately 750 gigabytes). Lateral per-pixel resolution was dependent on the objective: 0.551 μm (Olympus 25x, 1.05NA, water), 0.722 μm (Nikon 20x, 0.95NA, water), 0.740 μm (Nikon 20x, 0.45NA, ELWD, air) or z-steps of 2.28 μm with a lateral per-pixel resolution of 1.430 μm (Nikon 10x, 0.5NA, 5.5WD, glycerol).

Details of the ribbon scanning system are the same as described above in Section 2.4. In addition, the multiphoton volume acquired for this study used a Nikon A1 multiphoton, galvano line scanner with 2x averaging, 3 μm z-steps.

B.1.5 Image Reconstruction

Data store and processing infrastructure is the same as detailed in Section 2.5. Volume data sets ranged in size from 150-850GB. Mosaic images were assembled into volumes using Imaris File Converter. The volumes were manipulated in Imaris v4.0, configured to utilize 75% of the available RAM per workstation with the cache directory pointed to solid-state storage. Large volumes that required significant computational resources, for example the joining of the two independently imaged volumes, were completed on the computational server with Imaris

configured to use 450GB of RAM and the cache configured to use the 36TB RAID0 solid-state array.

B.1.6 Results

Large area acquisition is most useful in the context of deep volume imaging where whole tissues can be reconstructed in three dimensions. Depth imaging has historically been the domain of multiphoton microscopy which utilizes red-shifted ultrafast pulsed lasers and long working distance objectives to enhance tissue penetration. Conversely, depth penetration using conventional confocal imaging is limited to about 50 microns, due to a lack of light penetration into the tissue and a failure of the emitted light to pass through the confocal pinhole caused by scattering and absorbance. However, when either single or multiphoton systems are paired with tissue clearing protocols that match the refractive index of the tissue and remove light-refracting and light-absorbing molecules like lipids and chromophores (Becker, Jährling, Saghafi, Weiler, & Dodt, 2012b; Chung et al., 2013; Hama et al., 2011; Pan et al., 2016b; Renier et al., 2014b; Susaki et al., 2014b), imaging can be extended to multiple millimeter depths. When cleared tissue is used, the standard confocal microscope is generally more facile to use than multiphoton methods. The most compelling reason is the ability to image multiple concurrent channels with a broad spectrum of specific wavelengths. Using a long working distance multiphoton objective designed for deep tissue imaging (25x, 1.05NA, 2.0WD), we compared imaging in depth with the Caliber I.D. confocal (Fig. 5A) and a multiphoton (Fig. 5B) microscope. We found that, with tissue clearing, both methods allowed for imaging of cleared brain tissue at depths of two millimeters (the limit of the objective). In contrast to the multiphoton excitation, the Caliber I.D. confocal was more effective at distinguishing signal deep in the tissue. The cross-talk

observed between the 488 and 561 channels using the Caliber I.D. system was the result of simultaneous scanning, which is analogous to multiphoton where light is collected simultaneously. Simultaneous scanning was used for two-color ribbon-scanning in this study since the ribbon-scanning confocal experiences no change in the rate of acquisition while ribbon scanning.

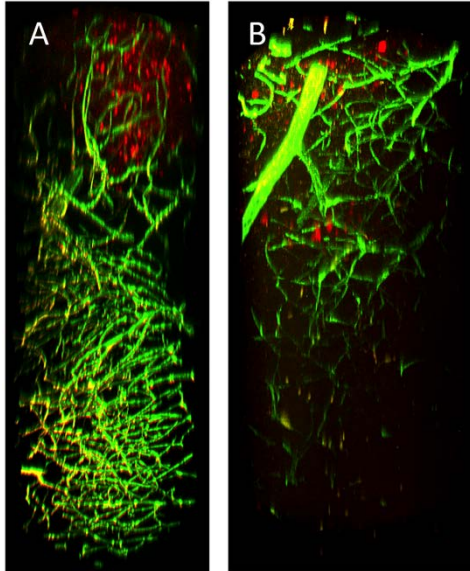


Figure 5. Confocal is more effective than 2-photon at multicolor deep tissue imaging in chemically cleared brains. A mouse was infected subcutaneously with VEEV TrD TaV-cherry (red) and at 96 hours post infection, fluorescent beads (green) were introduced into the vasculature by cardiac perfusion. The brain was harvested, sectioned approximately four millimeters thick, and cleared by CUBIC prior to imaging on the (A) Caliber I.D. ribbon scanning confocal and the (B) An Olympus XLPlan N 25X, 1.05NA objective was used to capture both volumes.

We then used the Caliber I.D. system to image through a cleared brain from a mouse infected with a GFP expressing alphavirus. The brain was embedded in hydrogel and coarsely sectioned to approximately 4mm thick prior to clearing by CUBIC. The area of each optical section was 21.0 x 15.5 millimeters acquired in z at 25.15 μ m intervals. The stitch for each z-

plane was determined based on the middle layer, which was acquired first, and that stitch was subsequently applied to all other layers. The resulting 3D reconstruction (Fig. 6A) took three hours and twenty minutes to complete and spanned 1735 microns in depth, approximately 1/4 of the mouse brain. Each optical plane (Fig. 6B) was acquired in 2.9 minutes with a resolution of approximately 551nm per pixel. Infected neurons were captured in subcellular detail throughout the volume (Fig. 6C-E), evidenced by the visualization of axons projecting from individually infected cells.

We then tested the utility of ribbon scanning for imaging large volumes and in multiple colors. A mouse was infected with a VEEV mCherry expressing virus and at the time of harvest we introduced green fluorescent beads into the vasculature by perfusion. Using the long working distance multiphoton objective, we imaged through one side of the section and then imaged again from the reverse side. Using simultaneous two color scanning, each optical section took 3.8 minutes to image, a total of 9.7 hours for both sides. The two images were joined into a single reconstructed volume representing approximately 1/2 of the mouse brain (4174 microns of tissue (Fig. 7A)). Each optical section displayed the full microvasculature within the tissue (Fig. 7B) as well as individually infected cells at subcellular resolution (Fig. 7C-D). We found that in many regions with strong virus replication, the microvasculature did not exhibit signal from the beads (Fig. 7D), a novel observation suggesting that virus replication may result in vascular destruction or occlusion.

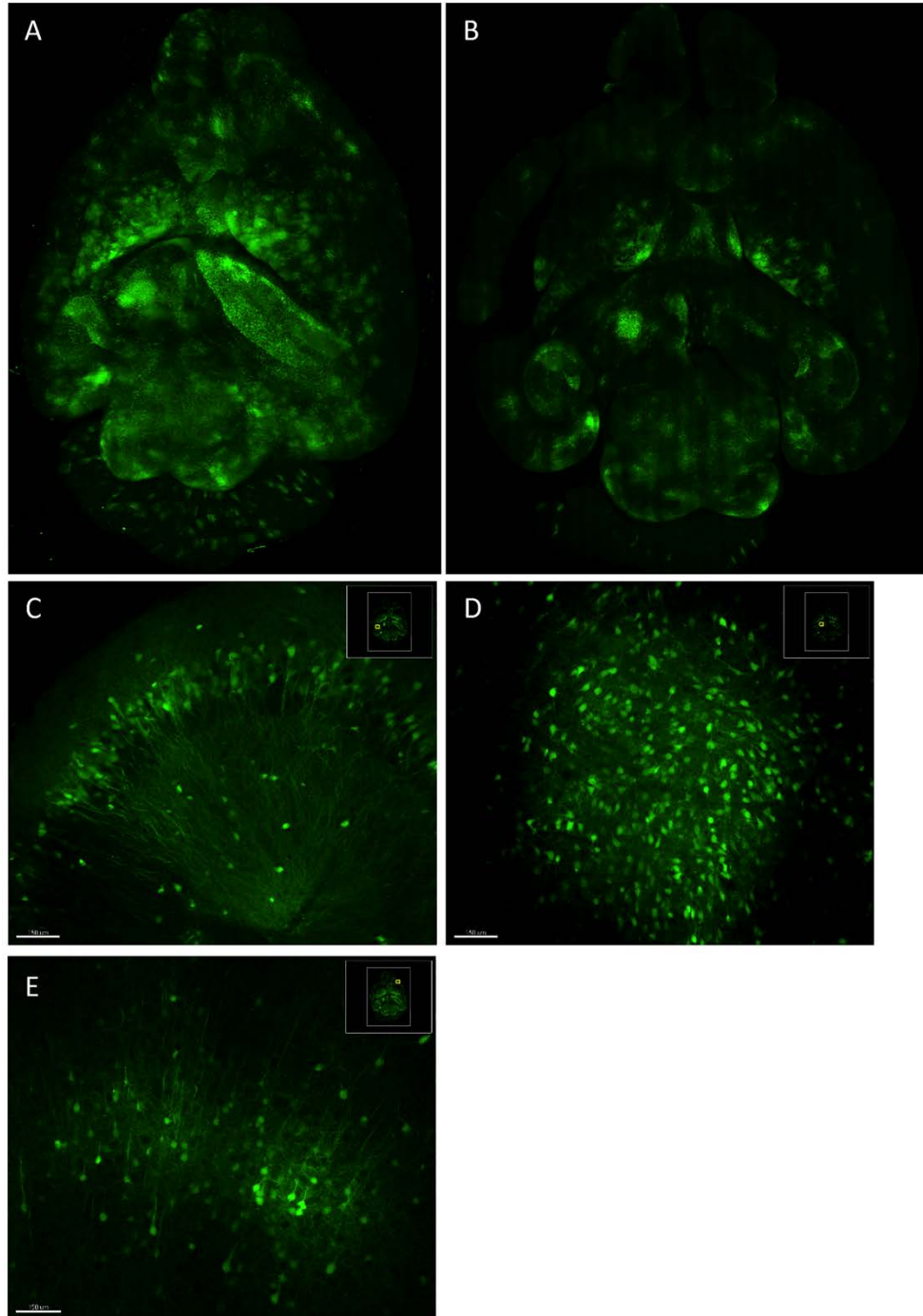


Figure 6. Ribbon scanning confocal microscopy captures subcellular detail throughout large volumes in chemically cleared mouse brains. A mouse was infected by aerosol with EEEV TaV-GFP. At 96 hours post infection, the brain was harvested, sectioned approximately four millimeters thick, and cleared by CUBIC. The Caliber I.D. ribbon scanning confocal was used to reconstruct a (A) 21.0 x 15.5 x 1.735 millimeter volume. (B) A single optical plane from the volume demonstrates the (C-D) subcellular detail captured throughout the volume.

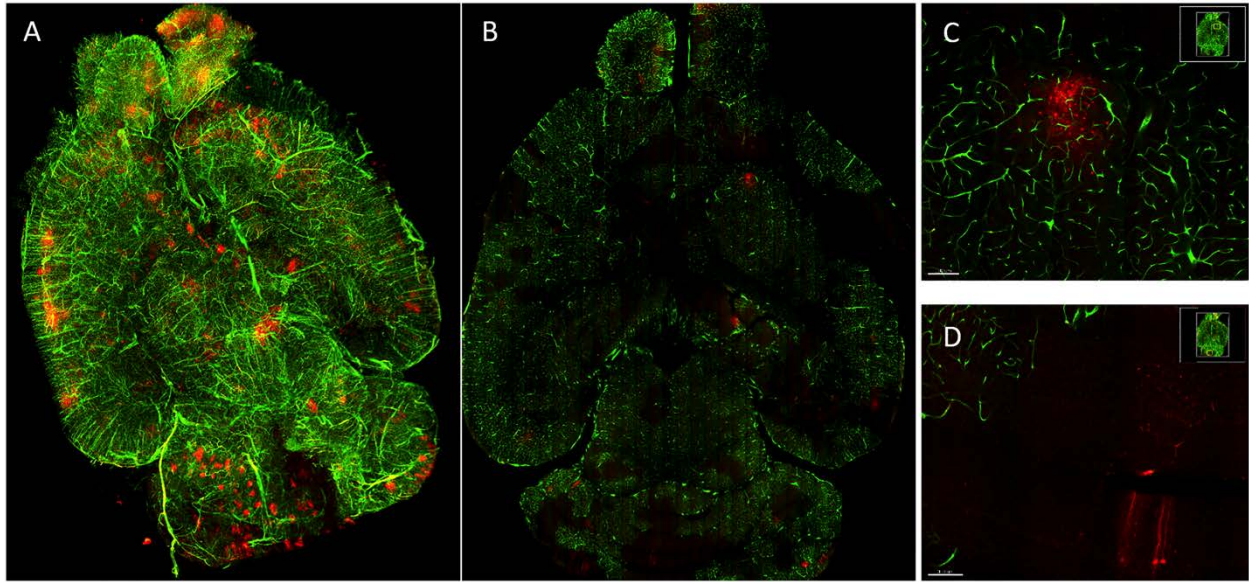


Figure 7. Multicolor large-volume imaging by ribbon scanning confocal microscopy. A mouse was infected subcutaneously with VEEV TrD TaV-cherry (red) and at 96 hours post infection, fluorescent beads (green) were introduced into the vasculature by cardiac perfusion. The brain was harvested, sectioned approximately four millimeters thick, and cleared by CUBIC. The section was imaged approximately two millimeters deep (the limit of the Olympus 25x, 1.05NA objective) on both sides and reconstructed as (A) on volume. (B) A single optical plane demonstrates that both the microvasculature and virus infected cells are observed throughout the volume. (C-D) Zoomed regions from a single optical place demonstrate in greater detail that the vasculature in some areas with virus replication are inaccessible to fluorescent beads administered by perfusion.

High NA multiphoton objectives are expensive and are commonly difficult to obtain without the purchase of a concomitant multiphoton system. To demonstrate that large volume imaging by ribbon scanning is plausible using more accessible objectives, we imaged the previous sample with a water immersion Nikon objective (20x, 0.95NA, 1.0WD) and a dry ELWD Nikon (20x, 0.45NA, 7.4WD). While there were obvious compromises in depth

penetration and signal recovery, due to working distance limitations or reduced NA, image quality remained high, and the resolution was sufficient to identify individual virus-infected cells and microvasculature. The working distance of the water immersion Nikon objective limited depth imaging to half that of the multiphoton objective and decreased the lateral resolution by 25% (722nm) per pixel, but the detail captured from this objective was visually comparable to the multiphoton objective including excellent signal recovery in deep tissue and subcellular and microvasculature detail. The ELWD Nikon 20x air objective is similar to those used on light-sheet systems capable of imaging whole mouse brains. Using this objective, we were able to acquire the whole tissue section in a single imaging session, requiring no computation to reconstruct the whole tissue as was required with the multiphoton lens in Fig. 5. The resulting images had a resolution similar to the 20x water lens (740nm per pixel), but signal originating from deep in the tissue appeared weak.

Finally, we used a new 10x, 0.5NA, 5.5WD objective designed by Nikon to acquire a sub-volume of a brain infected with Western Equine Encephalitis virus at a depth of 4.2 millimeters, 2.28 microns per slice (1850 z-slices) and 1430nm per pixel resolution. Individually infected neurons and the surrounding micro vasculature are visible throughout the volume. The volume represents approximately $\frac{1}{4}$ of a whole brain and required 17.7 hours to acquire at 30 seconds per optical slice. These data suggest that low magnification, high NA, long working distance objectives can be paired with ribbon scanning to image whole brains in under two days.

BIBLIOGRAPHY

- Becker, K., Jährling, N., Saghafi, S., Weiler, R., & Dodt, H.-U. (2012a). Chemical Clearing and Dehydration of GFP Expressing Mouse Brains. *PLoS ONE*, 7(3), e33916. <https://doi.org/10.1371/journal.pone.0033916>
- Becker, K., Jährling, N., Saghafi, S., Weiler, R., & Dodt, H.-U. (2012b). Chemical clearing and dehydration of GFP expressing mouse brains. *PloS One*, 7(3), e33916. <https://doi.org/10.1371/journal.pone.0033916>
- Bohland, J. W., Wu, C., Barbas, H., Bokil, H., Bota, M., Breiter, H. C., ... Mitra, P. P. (2009). A Proposal for a Coordinated Effort for the Determination of Brainwide Neuroanatomical Connectivity in Model Organisms at a Mesoscopic Scale. *PLoS Comput Biol*, 5(3), e1000334. <https://doi.org/10.1371/journal.pcbi.1000334>
- Bostan, A. C., Dum, R. P., & Strick, P. L. (2013). Cerebellar networks with the cerebral cortex and basal ganglia. *Trends in Cognitive Sciences*, 17(5), 241–254. <https://doi.org/10.1016/j.tics.2013.03.003>
- Cajal, S. R. y. (1891). Sur la structure de l'écorce cérébrale de quelques mammifères. *Typ. de Joseph van In & Cie.*
- Cajal, S. R. y. (1893). La rétine des vertébrés. *Typ. de Joseph van In & Cie.*

- Chung, K., Wallace, J., Kim, S.-Y., Kalyanasundaram, S., Andalman, A. S., Davidson, T. J., ... Deisseroth, K. (2013). Structural and molecular interrogation of intact biological systems. *Nature*, 497(7449), 332–337. <https://doi.org/10.1038/nature12107>
- De Carlos, J. A., & Borrell, J. (2007). A historical reflection of the contributions of Cajal and Golgi to the foundations of neuroscience. *Brain Research Reviews*, 55(1), 8–16. <https://doi.org/10.1016/j.brainresrev.2007.03.010>
- Dum, R. P., & Strick, P. L. (2003). An Unfolded Map of the Cerebellar Dentate Nucleus and its Projections to the Cerebral Cortex. *Journal of Neurophysiology*, 89(1), 634–639. <https://doi.org/10.1152/jn.00626.2002>
- Dum, R. P., & Strick, P. L. (2013). Transneuronal tracing with neurotropic viruses reveals network macroarchitecture. *Current Opinion in Neurobiology*, 23(2), 245–249. <https://doi.org/10.1016/j.conb.2012.12.002>
- Hama, H., Kurokawa, H., Kawano, H., Ando, R., Shimogori, T., Noda, H., ... Miyawaki, A. (2011). Scale: a chemical approach for fluorescence imaging and reconstruction of transparent mouse brain. *Nature Neuroscience*, 14(11), 1481–1488. <https://doi.org/10.1038/nn.2928>
- Helmstaedter, M., & Mitra, P. P. (2012). Computational methods and challenges for large-scale circuit mapping. *Current Opinion in Neurobiology*, 22(1), 162–169. <https://doi.org/10.1016/j.conb.2011.11.010>
- Hintiryan, H., Foster, N. N., Bowman, I., Bay, M., Song, M. Y., Gou, L., ... Dong, H.-W. (2016). The mouse cortico-striatal projectome. *Nature Neuroscience*, 19(8), 1100–1114. <https://doi.org/10.1038/nn.4332>

- Hoshi, E., Tremblay, L., Féger, J., Carras, P. L., & Strick, P. L. (2005). The cerebellum communicates with the basal ganglia. *Nature Neuroscience*, 8(11), 1491–1493. <https://doi.org/10.1038/nn1544>
- Kelly, R. M., & Strick, P. L. (2003). Cerebellar Loops with Motor Cortex and Prefrontal Cortex of a Nonhuman Primate. *The Journal of Neuroscience*, 23(23), 8432–8444.
- Levinthal, D. J., & Strick, P. L. (2012). The Motor Cortex Communicates with the Kidney. *The Journal of Neuroscience*, 32(19), 6726–6731. <https://doi.org/10.1523/JNEUROSCI.0406-12.2012>
- Majka, P., Chaplin, T. A., Yu, H.-H., Tolpygo, A., Mitra, P. P., Wójcik, D. K., & Rosa, M. G. P. (2016). Towards a comprehensive atlas of cortical connections in a primate brain: Mapping tracer injection studies of the common marmoset into a reference digital template. *Journal of Comparative Neurology*, 524(11), 2161–2181. <https://doi.org/10.1002/cne.24023>
- Middleton, F. A., & Strick, P. L. (2001). Cerebellar Projections to the Prefrontal Cortex of the Primate. *The Journal of Neuroscience*, 21(2), 700–712.
- Oh, S. W., Harris, J. A., Ng, L., Winslow, B., Cain, N., Mihalas, S., ... Zeng, H. (2014). A mesoscale connectome of the mouse brain. *Nature*, 508(7495), 207–214. <https://doi.org/10.1038/nature13186>
- Okano, H., & Mitra, P. (2015). Brain-mapping projects using the common marmoset. *Neuroscience Research*, 93, 3–7. <https://doi.org/10.1016/j.neures.2014.08.014>
- Okano, H., Miyawaki, A., & Kasai, K. (2015). Brain/MINDS: brain-mapping project in Japan. *Phil. Trans. R. Soc. B*, 370(1668), 20140310. <https://doi.org/10.1098/rstb.2014.0310>

- Pan, C., Cai, R., Quacquarelli, F. P., Ghasemigharagoz, A., Loubopoulos, A., Matryba, P., ... Ertürk, A. (2016a). Shrinkage-mediated imaging of entire organs and organisms using uDISCO. *Nature Methods*, advance online publication. <https://doi.org/10.1038/nmeth.3964>
- Pan, C., Cai, R., Quacquarelli, F. P., Ghasemigharagoz, A., Loubopoulos, A., Matryba, P., ... Ertürk, A. (2016b). Shrinkage-mediated imaging of entire organs and organisms using uDISCO. *Nature Methods*, 13(10), 859–867. <https://doi.org/10.1038/nmeth.3964>
- Reed, D. S., Bethel, L. M., Powell, D. S., Caroline, A. L., & Hartman, A. L. (2014). Differences in aerosolization of Rift Valley fever virus resulting from choice of inhalation exposure chamber: implications for animal challenge studies. *Pathogens and Disease*, 71(2), 227–233. <https://doi.org/10.1111/2049-632X.12157>
- Renier, N., Wu, Z., Simon, D. J., Yang, J., Ariel, P., & Tessier-Lavigne, M. (2014a). iDISCO: A Simple, Rapid Method to Immunolabel Large Tissue Samples for Volume Imaging. *Cell*, 159(4), 896–910. <https://doi.org/10.1016/j.cell.2014.10.010>
- Renier, N., Wu, Z., Simon, D. J., Yang, J., Ariel, P., & Tessier-Lavigne, M. (2014b). iDISCO: A Simple, Rapid Method to Immunolabel Large Tissue Samples for Volume Imaging. *Cell*, 159(4), 896–910. <https://doi.org/10.1016/j.cell.2014.10.010>
- Sun, C., Gardner, C. L., Watson, A. M., Ryman, K. D., & Klimstra, W. B. (2014). Stable, High-Level Expression of Reporter Proteins from Improved Alphavirus Expression Vectors To Track Replication and Dissemination during Encephalitic and Arthritogenic Disease. *Journal of Virology*, 88(4), 2035–2046. <https://doi.org/10.1128/JVI.02990-13>
- Susaki, E. A., Tainaka, K., Perrin, D., Kishino, F., Tawara, T., Watanabe, T. M., ... Ueda, H. R. (2014a). Whole-Brain Imaging with Single-Cell Resolution Using Chemical Cocktails

and Computational Analysis. *Cell*, 157(3), 726–739.
<https://doi.org/10.1016/j.cell.2014.03.042>

Susaki, E. A., Tainaka, K., Perrin, D., Kishino, F., Tawara, T., Watanabe, T. M., ... Ueda, H. R. (2014b). Whole-Brain Imaging with Single-Cell Resolution Using Chemical Cocktails and Computational Analysis. *Cell*, 157(3), 726–739.
<https://doi.org/10.1016/j.cell.2014.03.042>

Susaki, E. A., Tainaka, K., Perrin, D., Yukinaga, H., Kuno, A., & Ueda, H. R. (2015). Advanced CUBIC protocols for whole-brain and whole-body clearing and imaging. *Nature Protocols*, 10(11), 1709–1727. <https://doi.org/10.1038/nprot.2015.085>

Zingg, B., Hintiryan, H., Gou, L., Song, M. Y., Bay, M., Bienkowski, M. S., ... Dong, H.-W. (2014). Neural Networks of the Mouse Neocortex. *Cell*, 156(5), 1096–1111.
<https://doi.org/10.1016/j.cell.2014.02.023>